LANGMUIR
Article
Cite This: *Langmuir* XXXX, XXX, XXX−XXX
pubs.acs.org/Langmuir

Abnormal Rheological Phenomena in Newtonian Fluids in Electroosmotic Flows in a Nanocapillary

Jing Xue,[†] Wei Zhao,[*,†] Ting Nie,[†] Ce Zhang,[†] Shenghua Ma,[†] Guiren Wang,[†,‡] Shoupeng Liu,[§] Junjie Li,[∥] Changzhi Gu,[∥] Jintao Bai,[†] and Kaige Wang[*,†]

[†]State Key Laboratory of Cultivation Base for Photoelectric Technology and Functional Materials, Laboratory of Optoelectronic Technology of Shaanxi Province, National Center for International Research of Photoelectric Technology & Nanofunctional Materials and Application, Institute of Photonics & Photon-Technology, Northwest University, Xi'an 710069, China

[‡]Department of Mechanical Engineering & Biomedical Engineering Program, University of South Carolina, Columbia, South Carolina 29208, United States

[§]Suzhou Institute of Biomedical Engineering and Technology, Chinese Academy of Sciences, Suzhou 215163, China

[∥]Institute of Physics, Chinese Academy of Sciences, Beijing 100190, China

S *Supporting Information*

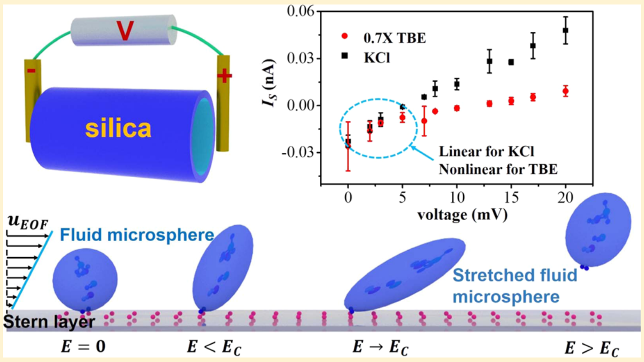

ABSTRACT: Abnormal rheological phenomena arising in Tris-borate−ethylenediaminetetraacetic acid solutions (believed to be Newtonian fluids) were observed in direct current electroosmotic flows within a nanocapillary with a diameter of 200 nm under a low electric field of tens of volts per meter. In solutions with different concentrations and pH values, the flow behavior indices of the power-law fluids were calculated on the basis of current−voltage relations. When the electric field intensity was below a critical value of 6.7 V/m, the fluids exhibited dilatant (shear thickening) effects. Fluid viscosity changed with electric field intensity because the near-wall shear rate of an electroosmotic flow changes with electric field intensity via a power-law relation. When the electric field intensity surpasses the critical electric field, the fluid again becomes Newtonian and has constant viscosity. The investigation shows that in nanocapillaries, fluids commonly believed to be Newtonian can become non-Newtonian near walls as a result of strong nanoscale interfacial effects. The results can also improve our understanding of electroosmosis-related transport phenomena in nanofluidics and biomedical science.

INTRODUCTION

Fluid flows in nanocapillaries and the corresponding transport phenomena of ions, particles, and biomolecules have attracted intensive attention in fluid dynamics and the life sciences. Many new phenomena have been observed in nanofluidics.[1] In 1990, Pfahler et al.[2] found that the flow rates of *n*-propanol in a submicrochannel can be 3 times greater than expected. Later, Majumder et al.[3] experimentally observed that abnormally high flow rates can be realized in nanotubes with a diameter of 7 nm, implying the existence of a wall-slip phenomenon in nanoflows. In nanofluidics, due to the large surface-to-volume ratio, surface effects become dominant, as in ionic transport. Stein et al.[4] studied ion transport in nanocapillaries under controlled surface charge and found that at the dilute limit, the conductance saturation values of channels were independent of both the salt concentration and channel height. Therefore, the electric conductance of nanocapillaries falls into two regimes. At low ionic concentrations, conductance is governed by surface charge, whereas at high ionic concentrations, conductance is determined by both nanocapillary geometry and bulk ionic concentration. Kneller et al.[5] also observed a directional dependency of electric conductivity in asymmetric nanocapillaries.

In biomedical and life science research, electrokinetic flows produced by or occurring within living organisms not only rely on the cell membrane net charge (polarization) but also induce variations in local biophysical and chemical properties at the nanometer scale along the membrane surfaces of single cells, which in turn triggers the downstream signaling pathways.[6,7] The effects of bioelectricity on fluids and surface characteristics at the nanoscale, although important, remain poorly understood. For example, in our previous investigation,[8] we observed a sudden fall-off in electric conductance in a nanocapillary with a diameter of 200 nm. This phenomenon was attributed to the shear-thickening effect of a Tris-borate−ethylenediaminetetraacetic acid (EDTA) (TBE) solution under a direct current

Received: September 12, 2018
Revised: November 2, 2018
Published: November 12, 2018

DOI: 10.1021/acs.langmuir.8b03112

(DC) electric field, i.e., a kind of rheological effect. In this study, we systematically investigated the rheological behavior of TBE solution (which was believed to be a Newtonian fluid) in a nanofluidic channel by studying current−voltage relations. An abnormally nonlinear current−voltage relation was first observed at a low electric field. In contrast, normally nonlinear current−voltage phenomena always appear at high electric fields. The nonlinear current−voltage relations in this investigation revealed abnormal rheological phenomena in electroosmotic flows (EOFs) under low DC electric fields. The phenomena were new since even if there exists electrorheological effect, it normally requires a strong electric field, for instance, beyond 10^6 V/m^9.[9] This new observation may aid in modeling cellular environments in vivo for biological and medical studies.

EXPERIMENTAL SETUP AND PROCEDURE

The experimental setup is schematically shown in Figure 1. A nanocapillary with a circular cross section, a length of 3 mm and an inner diameter (D) of 200 nm, was used to connect two reservoirs on both sides, as shown in Figure 1a. The nanocapillary was made of silicon nitride. The two reservoirs were composed of poly(tetrafluoroethylene), which exhibits excellent dielectric, chemical, and mechanical stability.[10] One was named the cis chamber, and the other was named the trans chamber. Both reservoirs had the same dimensions.

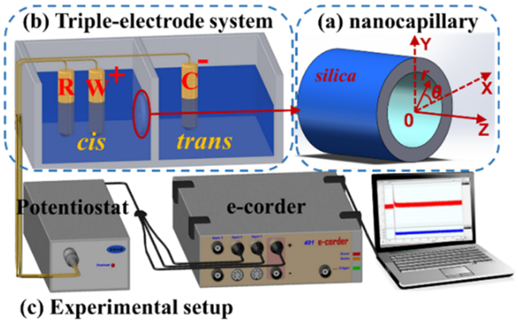

Figure 1. Schematic of the experimental setup used in this investigation. (a) Structure of the nanocapillary represented in a cylindrical coordinate system. (b) The triple-electrode system, where "W" represents the working electrode and "R" is the reference electrode. Both the working electrode and reference electrode are placed into the cis chamber. "C" represents the counter electrode, which is placed inside the trans chamber. (c) Instruments used for the experiment.

A triple-electrode measurement system was used in the experiments, as shown in Figure 1b. Both the working electrode (anode) and reference electrode were inserted into the cis chamber, and the counter electrode (cathode) was inserted into the trans chamber. All the electrodes were made of Pt. In this research, a reference electrode was inserted into the cis chamber to construct a triple-electrode measurement system and to provide a reference signal for the working electrode. Compared with the current response in the conventional two-electrode method, the triple-electrode measurement system recovers more quickly, which can improve the stability of measurements. The cathode area (S_C) was 20 times greater than the anode area (S_W). The area ratio (S_C/S_W) between the cathode and anode was consistent with that used by Duan et al.,[8] who showed an interesting and abnormal "fall-off" in electric conductance. This is why an area ratio of 20 was used in the subsequent investigation.

A precise potentiostat (EA162, eDAQ, Australia) was used to provide accurate and stable voltage, and a microcurrent detector (EA162, e-corder 401, eDAQ, Australia) was used to monitor the weak current signals, as shown in Figure 1c. To shield external electromagnetic noise, a grounded Faraday cage was used during the measurements. The experiments were carried out at 25 °C to avoid the influence of temperature fluctuations.

In the experiments, the working fluid was a TBE buffer solution that was prepared with Tris (tris(hydroxymethyl)aminomethane, an organic compound with the chemical formula $(HOCH_2)_3CNH_2$), boric acid (borate), and ethylenediaminetetraacetic acid disodium salt (EDTA-2Na, an aminopolycarboxylic acid). The concentrations (C_{TBE}) of the TBE buffer were 0.3×, 0.5×, 0.7×, 1×, and 2×. The corresponding concentrations of each component are listed in Table 1. The influence of the pH value (6, 7, 8, and 9) of the solutions was also taken into account. The pH values of the solutions were controlled by adding HCl or NaOH.

Table 1. Experimental conditions

	concentration		
C_{TBE}	EDTA-2Na (mM)	borate (mM)	Tris (mM)
0.3×	0.6	26.69	20.56
0.5×	1	44.48	34.26
0.7×	1.4	62.27	47.97
1×	2	88.95	68.53
2×	4	177.9	137.1

The viscosity of bulk TBE buffer solution was measured by a rheometer (HAAKE Mars60, Germany). As shown in Figure 2a, in the considered range of shear rates (γ), the dynamic viscosity (η) of the fluid remained almost unchanged at approximately 1 mPa s. The flow behavior index (also known as the power-law index, n)[11] of the fluid was also investigated, as plotted in Figure 2b. For the five concentrations of TBE solution, all of the measured n values were sufficiently close to 1. Both Figure 2a,b clearly indicate that the bulk TBE buffer solutions from 0.3× to 2× were Newtonian fluids. However, this conclusion no longer stands in nanofluidics, as shown later.

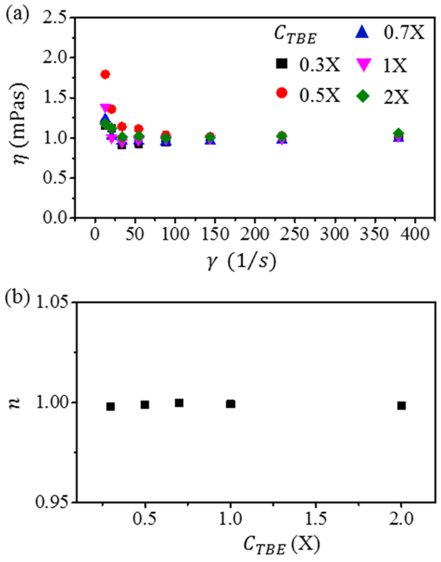

Figure 2. Viscosity and flow behavior index of TBE buffer solution with different concentrations (0.3×, 0.5×, 0.7×, 1×, and 2×). pH = 8. (a) Viscosity vs shear rate. (b) Flow behavior index vs concentration of TBE buffer solution.

To explore how current is affected by the solution parameters, we systematically studied the current signals of the TBE buffer solutions in the nanocapillary. Details of the experimental conditions are listed in Table 2.

Table 2. Experimental conditions

parameters	values
solution types	TBE buffer and KCl
C_{TBE}	0.3×, 0.5×, 0.7×, 1×, 2×
debye length (λ) (nm)	0.2−0.6
voltage change (mV)	0, 3, 5, 7, 8, 10, 13, 15, 17, 20, 25, ..., 45, 50
pH	6, 7, 8, 9

The experimental procedure is briefly described as follows. First, a reservoir was filled with TBE buffer solution. By capillary force, the solution was drawn into the nanocapillary. Immediately after the capillary was completely filled with the solution, the same solution was added to another reservoir. During the injection, we carefully ensured that the buffer solution flowed into the nanocapillary and no air bubbles or contaminants were present. Second, the working electrode, reference electrode, and counter electrode were inserted into the cis and trans chambers. When the electrodes were connected to the potentiostat and current detector, the entire system was placed in the Faraday electromagnetic cage. Finally, after a DC voltage was applied, the current measurements were started. For each measurement, 2 min were normally required to stabilize the current. The sampling process was then carried out in 5 min. To ensure reliable measurements, in each case, the experiments were repeated four to five times to take the ensemble average. After each experiment, the nanocapillary was soaked with deionized (DI) water for 30 min and then cleaned in an ultrasonic cleaner for 10 min. When the experiments were completed, the channel system and electrodes were placed in DI water for 2 h to eliminate residues. After the completion of all of the steps, the channel system was kept in DI water. All experiments were carried out at room temperature (25 °C).

■ EXPERIMENTAL RESULTS

Nonlinear Current−Voltage Relations. In our experiments, the voltage (V) between the two electrodes ranged from 0 to 50 mV. The equivalent electric field intensities (E) were 0−16.7 V/m. Two solutions (KCl and 0.7× TBE) with the same bulk conductivities and pH values were studied first. As shown in Figure 3, although in bulk solution, the KCl (30−50 mM, depending on the pH value) and 0.7× TBE solutions exhibit equivalent electric conductivities, in the nanocapillary, the local electric conductance, which is denoted by the slope of the steady current (I_s)—voltage (V) curve, can differ greatly. The KCl solution always exhibits higher electric conductance than the 0.7× TBE solution. Surprisingly, when the pH value is 6 (as shown in Figure 3a), the I_s-V curves of both solutions are still linear. However, as plotted in Figure 3b, when the pH value is increased to 7, although the KCl solution maintains a linear I_s-V relation, the I_s-V curve of the 0.7× TBE solution becomes apparently nonlinear in the low-voltage regime, where $V \leq 20$ mV (the equivalent electric field intensity was 6.7 V/m). When the pH value is increased to 9, in Figure 3c, the I_s-V curve of the 0.7× TBE solution becomes higher and nonlinear. Similar nonlinear phenomena were also found for nanochannels in the investigation of Singh and Guo.[12] Due to the application of unbalanced electrodes, a bias current I_{s_0} can be observed in almost all of the experiments. However, a bias current cannot lead to a nonlinear I_s-V curve. Therefore, in the subsequent analysis, the influence of I_{s_0} will not be taken into account.

The current values for the TBE buffer solutions with different concentrations at pH = 7 were measured in the nanocapillary later. The results are shown in Figure 4. An apparently nonlinear I_s-V relation was observed for the TBE buffer solution when $V \leq 20$ mV (the equivalent electric field intensity was 6.7 V/m). On the basis of the variation in the I_s-V curve from nonlinear to linear, the I_s-V plot can be separated into two subregions, which are subregion I at $V \leq 20$ mV and subregion II at $V > 20$ mV, as plotted in Figure 4a. In subregion I, I_s-V was typically nonlinear. In subregion II, however, I_s-V recovered linear behavior, and Ohmic law remained valid for that region. This nonlinearity was also observed in Figure 4b for different TBE concentrations. Figure 4c shows that the two subregions exhibit different electric conductance. The magnitude of electric conductance in subregion I is apparently higher than that in subregion II. This is consistent with our previous investigations.[8] Similar two-subregion behaviors of the I_s-V relation were also observed under pH = 6, 8, and 9, as shown in Figure 5.

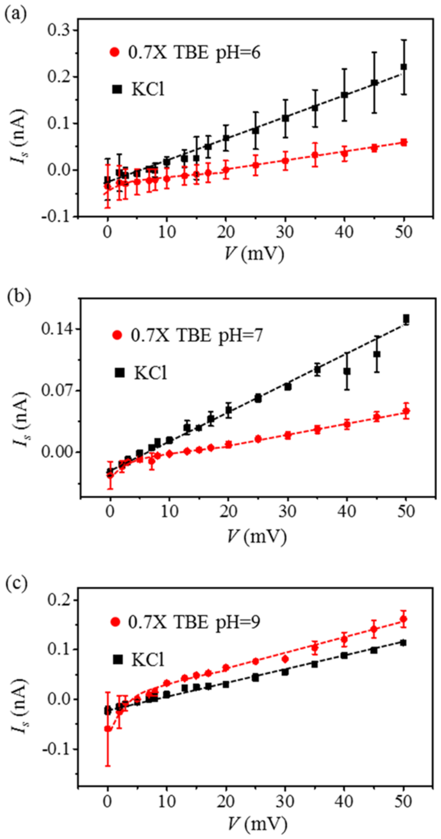

Figure 3. I_s-V curves for two solutions (KCl and 0.7× TBE) with the same bulk conductivities and pH values. (a), (b), and (c) represent pH values of 6, 7, and 9, respectively.

From both Figures 4 and 5, the nonlinear behavior of I_s-V in subregion I was strongly related to the TBE concentration and the pH value. When the concentration of the TBE solution was increased, the slope of I_s-V increased in subregion II, as expected, due to the solution's increasing bulk conductivity. However, the curvature of the I_s-V curve in subregion I did not vary monotonically with TBE solution concentration. A minimum curvature was reached at 0.7× TBE. At the other concentrations, the curvatures of the I_s-V curves increased again.

The nonlinear behavior of I_s-V is astonishing because most of the nonlinear I_s-V relation occurs under a much stronger electric field and bends concavely due to the nonlinear electrical double layer (EDL) on electrodes. This new observation implies that transport phenomena under a low electric field are not well understood. Our previous investigations[8] implied that near-wall fluids may exhibit rheological behavior; that is, the flow was locally non-Newtonian. This model can perfectly explain our observations of the nonlinear I_s-V curve in this manuscript, as shown below.

I_s-V Relation of Non-Newtonian Fluids. In general, a steady current (I_s) can be described by the overall effect of bulk conductance ($I_{s,c}$) and streaming current ($I_{s,s}$), i.e., $I_s = I_{s,c} + I_{s,s}$. In a channel of circular cross section and when the streaming current is caused by only electroosmotic flows, as investigated by Keh and Liu (1995),[13] we have

$$I_{s,c} = H_{s,c}E \tag{1}$$

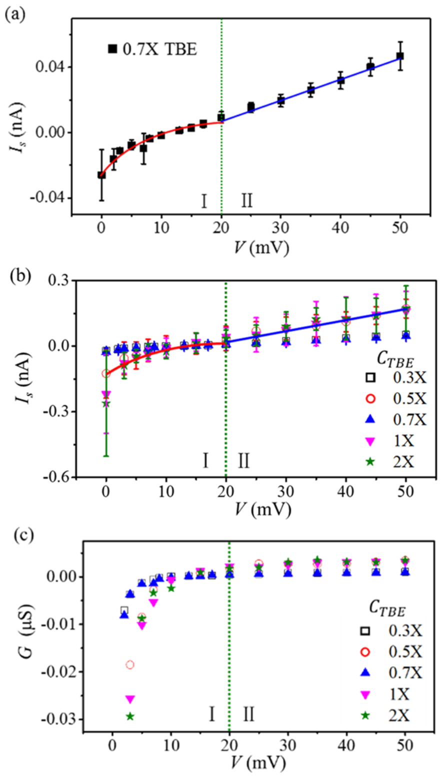

Figure 4. I_s−V curves and electric conductance of the TBE buffer solutions in a nanocapillary at pH = 7. (a) Original I_s−V relation in 0.7× TBE buffer solution. (b) I_s−V relations for TBE buffer solutions of different concentrations. In the diagram, the concentrations are 0.3×, 0.5×, 0.7×, 1×, and 2×. (c) The conductance (G)−voltage relations for TBE buffer solutions of different concentrations.

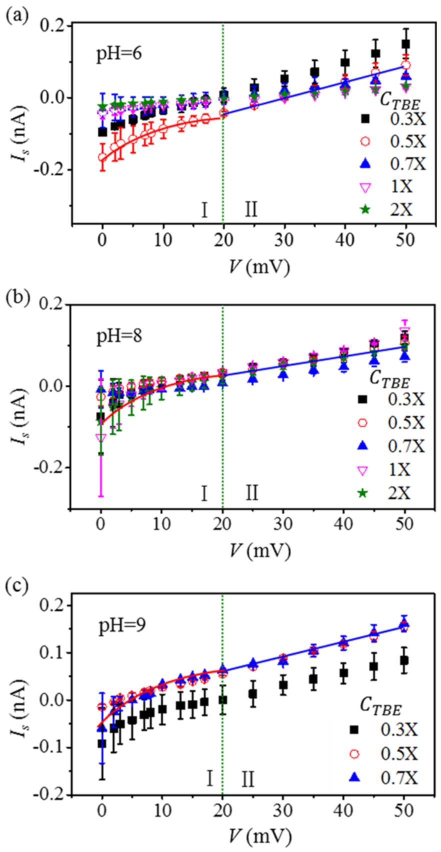

Figure 5. I_s−V curves of the TBE buffer solutions in a nanocapillary at different pH values. (a), (b), and (c) represent pH values of 6, 8, and 9, respectively. The red line is plotted to exhibit the nonlinear curve in subregion I.

$$I_{s,s} = H_{s,s}E/\eta \tag{2}$$

with

$$H_{s,c} = \pi R^2\left[\sigma - \frac{2}{k_B T}\frac{\varphi}{\kappa R I_0(\kappa R)} I_1(\kappa R)\sum_i q_i^3 e^3 C_i b_i\right] \tag{3}$$

$$H_{s,s} = \frac{\varepsilon^2\kappa^2 R^2}{16\pi}\frac{\varphi^2}{I_0^2(\kappa R)}\left[I_1^2(\kappa R) - I_0^2(\kappa R) + \frac{2}{\kappa R}I_0(\kappa R)I_1(\kappa R)\right] \tag{4}$$

where R is the radius of the nanocapillary; E is the magnitude of the electric field in the nanocapillary; $\sigma = \sum_i q_i^2 e^2 C_i b_i$ is the electric conductivity of TBE solution; q_i, C_i, and b_i are the electric valence, ionic concentration, and mobility, respectively, of the ith ion; e is the electron charge; $\kappa = 1/\lambda$ is the reciprocal of the Debye length; $\lambda = \sqrt{\varepsilon k_B T/4\pi\sum_i q_i^2 e^2 C_i}$, where $\varepsilon = \varepsilon_0\varepsilon_r$ is the electric permittivity of the medium, with ε_0 and ε_r being the vacuum and relative permittivity, respectively; k_B is Boltzmann's constant; T is the temperature; and φ is the surface potential, which is equal to the zeta potential ζ.[14] Parameters I_0 and I_1 are the zeroth- and first-order modified Bessel functions of the first kind, respectively.

From eq 3, it can be seen that $H_{s,c}$ is primarily determined by geometrical parameters (κR and R) and ionic parameters, such as ionic concentration, valence, and mobility. All these parameters are irrelevant to the applied electric field $E = V/L$ (L is the length of the nanocapillary). Similarly, in eq 4, κR, ε, and φ are all independent of E. Therefore, $H_{s,s}$ is also irrelevant to E. Thus, the nonlinear I_s−V curve investigated in this manuscript cannot be caused by $H_{s,c}$ and $H_{s,s}$. η becomes the only factor that may lead to the nonlinear I_s−V curve, even though η is almost constant in bulk TBE solutions, as shown in Figure 2. This is not beyond expectation. From Table 2, λ is between 0.2 and 0.6 nm in this investigation. The equivalent κR ranges from 167 to 500, which is much larger than unity. The strong interfacial effect of EDL and a large γ may lead to unexpected rheological effects (see the Discussion for details) and a nonconstant η, when γ is changed due to changing E.

In non-Newtonian fluids, generally, η is related to the shear strain rate $\gamma = du/dr$ as $\eta = K\gamma^{n-1}$,[11] where r represents the radial coordinate, K is the flow consistency index, and n is the flow behavior index. When an EOF is generated by a DC electric field, the velocity of the EOF at the outer edge of an electrical double layer can be approximated with the Helmholtz−Smoluchowski velocity, i.e., $u_{HS} = \varepsilon|\zeta|E/\eta$. Here, E is nonarbitrarily assumed to be positive for theoretical analysis.

Because the thickness of the EDL was normally less than 10 nm in this investigation, the EDL was much thinner than the transverse size of the nanocapillary. We can linearly approximate the velocity profile within the EDL; then, $\gamma \approx u_{HS}/\lambda$. By substituting u_{HS} and γ into η, we easily obtain $\eta = K(\varepsilon|\zeta|E/\eta\lambda)^{n-1}$. This equation leads to

$$\eta = K^{1/n}\left(\frac{\varepsilon|\zeta|E}{\lambda}\right)^{n-1/n} \tag{5}$$

After eq 5 is substituted into eq 2, $I_{s,s}$ becomes

$$I_{s,s} = \frac{\varepsilon^{n+1/n}\kappa^2 R^2\lambda^{n-1/n}|\zeta|^{1+n/n}}{16\pi K^{1/n} I_0^2(\kappa R)}\left[I_1^2(\kappa R) - I_0^2(\kappa R) + \frac{2}{\kappa R}I_0(\kappa R)I_1(\kappa R)\right]E^{1/n} \tag{6}$$

Considering that $I_s = I_{s,c} + I_{s,s}$, we finally have

$$I_s = B_1 V + B_2 V^{1/n} + I_{s_0} \tag{7}$$

where

$$B_1 = \frac{\pi R^2}{L}\left[\sigma - \frac{2}{k_\mathrm{B}T}\frac{\zeta}{\kappa R I_0(\kappa R)} I_1(\kappa R) \sum_i q_i^{\,3} e^3 C_i b_i\right] \tag{8}$$

$$B_2 = \frac{\varepsilon^{n+1/n}\kappa^2 R^2 \lambda^{n-1/n} |\zeta|^{1+n/n}}{16\pi K^{1/n} I_0^2(\kappa R) L^{1/n}}\left[I_1^2(\kappa R) - I_0^2(\kappa R) + \frac{2}{\kappa R} I_0(\kappa R) I_1(\kappa R)\right] \tag{9}$$

are the parameters that are irrelevant to the applied voltage. I_{s_0} denotes the current when V approaches zero.

Flow Behavior Index for Different Solution Concentrations and pH Values. The flow behavior index n can be obtained via nonlinear fitting of the experimental data using eq 7 via MATLAB software, as shown in Figure 6 (see Supporting Information for more details). For instance, in the 0.7× TBE buffer solution, n first increases with the pH value and reaches a maximum at pH = 7. Then, n slightly falls off. Nevertheless, under a pH value of 7, n increases with the concentration (C_{TBE}) of TBE buffer solution until n = 3.16, when C_{TBE} = 1×. After that, n slightly drops to 2.65 when C_{TBE} is increased to 2×. The n in nanofluidics driven by an electric field is clearly different from that of bulk solution, as plotted in Figure 2.

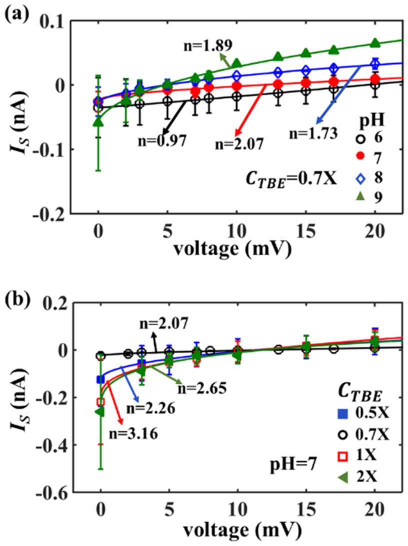

Figure 6. Nonlinear I_s−V curves fitted by eq 7 to calculate the flow behavior index n. (a) The concentration of TBE buffer solution is 0.7×. Four pH values, i.e., 6, 7, 8, and 9, are investigated. (b) The pH of the TBE buffer solutions is 7, and the concentrations are 0.5×, 0.7×, 1×, and 2×.

The results of nonlinearly fitted n are plotted in Figure 7. The parameter n varied with both pH and TBE solution concentration in a divergent manner. As shown in Figure 7a, most of the values of n exceed 1, which indicates a slight dilatant (i.e., shear thickening) behavior of the fluid under a low electric field. Under pH values of 6, 7, and 8, the maximum n values all appear at C_{TBE} = 1×, as indicated by the dashed circle. At this concentration, n can be as large as 3.2. From Figure 6a, the n at pH ≈ 7 is almost always higher than those at other pH values. This is more visible in Figure 7b, as highlighted by the dashed circle. Generally, more acidic or alkaline solutions (e.g., pH = 6 or 9) show weaker rheological features. The rheology of the fluid near the wall was substantially inhibited by the higher concentration of H^+ or OH^- ions, as represented by the smaller n. Neutral solutions experience stronger rheology near the wall, especially in or around the EDL.

Relation between n and Shear Stress. The results above indicate that in a neutral solution, there could be unexpected apparently rheological feathers in the flows. The variation in viscosity with electric field is schematically plotted in Figure 8a. For n values greater than unity, η increased more rapidly with E, as n increased. In addition, $u_{\mathrm{HS}} \approx (\varepsilon\xi E K^{-1}\lambda^{n-1})^{1/n}$ indicates a fractional power law between u_{HS} and the applied electric field, as plotted in Figure 8b. Larger n values are always accompanied by slower increases in u_{HS} with increasing E. Because TBE solutions with pH values of approximately 7.3 are widely used when preparing biochemical and biomedical samples for microfluidic/nanofluidic applications, the rheological effect must be taken into account because the wall shear stress can be significantly enhanced. This trend can be shown with one-dimensional and steady-flow approximations of the Navier–Stokes equation in a cylindrical coordinate system, as[13]

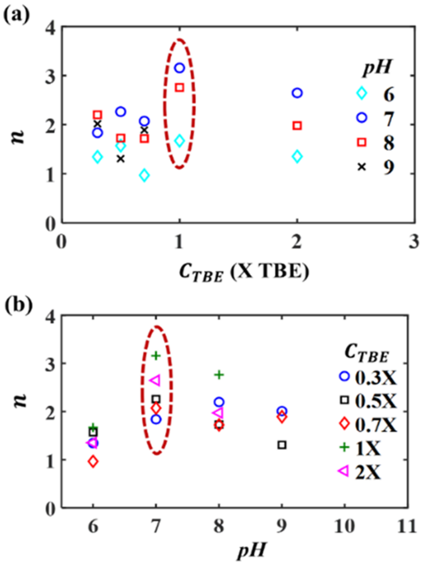

Figure 7. Variation in the flow behavior index n with pH for different concentrations (C_{TBE}) of TBE solution. (a) Influence of C_{TBE} on n. The C_{TBE} values with the highest n for different pH values are highlighted by dashed circles. (b) Influence of the pH value on n. The pH values with the highest n for different C_{TBE} values are highlighted by dashed circles.

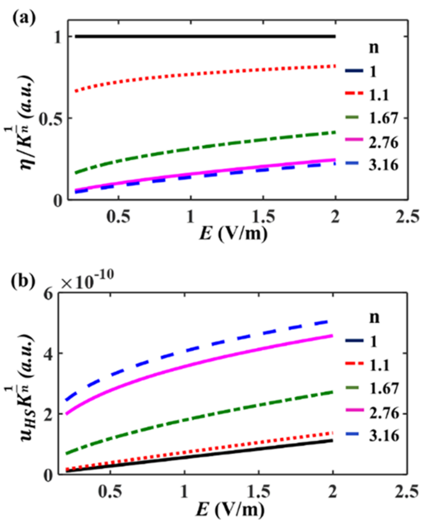

Figure 8. Variation in viscosity and u_{HS} with E and n for a 1× TBE solution. (a) The normalized viscosity $\eta/K^{1/n}$ plotted against E for different n values. (b) The normalized u_{HS} with $u_{\mathrm{HS}}K^{1/n}$ plotted against E for different n values.

DOI: 10.1021/acs.langmuir.8b03112
Langmuir XXXX, XXX, XXX−XXX

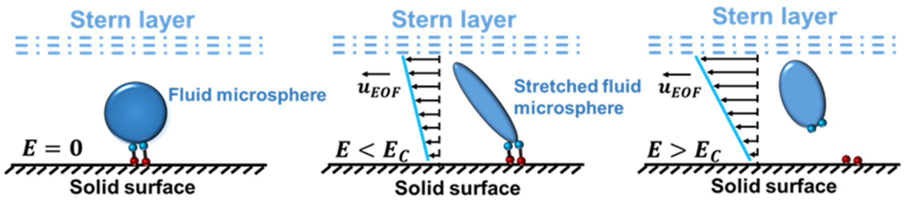

Figure 9. Schematic of the rheological phenomenon under a low electric field near the sidewall.

$$\frac{1}{r}\frac{\mathrm{d}}{\mathrm{d}r}\left(r\eta\frac{\mathrm{d}u}{\mathrm{d}r}\right) + \rho_e E = 0 \tag{10}$$

where

$$\rho_e = -\frac{\varepsilon\kappa^2 I_0(\kappa r)\zeta}{4\pi I_0(\kappa R)} \tag{11}$$

is the charge density distribution. Here, we focus on the shear stress near the wall, i.e., $\kappa(R - r) < 1$. Because the EDL was much thinner than the channel radius in this investigation, $\kappa R \gg 1$. Thus, we have the following approximations

$$I_0(\kappa r) \approx \mathrm{e}^{\kappa r}/\sqrt{2\pi\kappa r} \tag{12}$$

$$I_0(\kappa R) \approx \mathrm{e}^{\kappa R}/\sqrt{2\pi\kappa R} \tag{13}$$

Then

$$\frac{I_0(\kappa r)}{I_0(\kappa R)} \sim \frac{\mathrm{e}^{\kappa r}/\sqrt{2\pi\kappa r}}{\mathrm{e}^{\kappa R}/\sqrt{2\pi\kappa R}} = \mathrm{e}^{\kappa(r-R)}\sqrt{R/r} \tag{14}$$

Considering $\kappa(R - r) < 1$, by Taylor expansion

$$\mathrm{e}^{\kappa(r-R)} = 1 - \kappa(R - r) + \frac{[\kappa(R - r)]^2}{2} \tag{15}$$

In addition, by applying binomial expansions on $\sqrt{R/r}$, we have

$$\sqrt{R/r} = \frac{1}{\sqrt{1 - \frac{R-r}{R}}} \approx 1 + \frac{R - r}{2R} + \frac{3(R - r)^2}{8R^2} \tag{16}$$

After approximating to the first order of $R - r$, we have

$$\frac{I_0(\kappa r)}{I_0(\kappa R)} \approx 1 - \kappa(R - r) + \frac{\kappa(R - r)}{2\kappa R} \tag{17}$$

In addition, given $\kappa R \gg 1$, we finally obtain

$$\rho_e \approx -\frac{\varepsilon\kappa^2\zeta[1 - \kappa(R - r)]}{4\pi} \tag{18}$$

After substituting $\eta = K\gamma^{n-1}$, γ, and ρ_e into eq 10, we have

$$\frac{1}{r}\frac{\mathrm{d}}{\mathrm{d}r}(r\gamma^n) = \frac{\varepsilon\kappa^2\zeta E}{4\pi K}[1 - \kappa(R - r)] \tag{19}$$

Furthermore, ignoring the sign of ζ and only considering the magnitude of γ, the solution of eq 19 becomes

$$\gamma = \left[\frac{\varepsilon\kappa^2|\zeta|E}{4\pi K}\left(\frac{1 - \kappa R}{2}r + \frac{\kappa r^2}{3}\right) + \frac{B_3}{r}\right]^{1/n} \tag{20}$$

When $E = 0$, $\gamma = 0$; thus, $B_3 = 0$. Then

$$\gamma = \left[\frac{\varepsilon\kappa^2|\zeta|E}{4\pi K}\left(\frac{1 - \kappa R}{2}r + \frac{\kappa r^2}{3}\right)\right]^{1/n} \tag{21}$$

with the maximum γ, $\gamma_{\max} = \left[\frac{\varepsilon\kappa^2|\zeta|E}{8\pi K}\left(1 - \frac{\kappa R^2}{3}\right)\right]^{1/n}$, located at the wall. The magnitude of near-wall shear stress can be accordingly expressed as

$$\tau = \eta\gamma = \frac{\varepsilon\kappa^2|\zeta|E}{4\pi K}\left(\frac{1 - \kappa R}{2}r + \frac{\kappa r^2}{3}\right) \tag{22}$$

The maximum τ, i.e.,

$$\tau_{\max} = \frac{\varepsilon\kappa^2|\zeta|E}{8\pi K}\left(1 - \frac{\kappa R^2}{3}\right) \tag{23}$$

is also located on the wall. Interestingly, τ has a quadratic distribution along the radial direction but is independent of n. That is, the distribution of shear stress in the region of EDL is unaffected by the rheological nature of the solution. Relative to $\tau_{\max}$, $\gamma_{\max}$ has fractal scaling exponents of r and E.

■ DISCUSSION AND CONCLUSIONS

To date, the cause of the shear-thickening effect of TBE solution in nanochannels at low electric fields remains unclear. The interaction between the TBE molecules and the wall of the nanocapillary through multiple intermolecular forces on the surfaces, e.g., Hamaker attraction and van der Waals forces, might be responsible for the shear-thickening effect.[15] The transition of the fluid's flow property from non-Newtonian to Newtonian can be explained as diagrammed in Figure 9. When $E = 0$, the fluid particle remains in an equilibrium state. The strong intermolecular forces between the polarized wall and TBE molecules form relatively stable and ordered layers of TBE molecules. This is similar to the findings of Feng et al.[16] on the EDL of organic solutions. After the application of a small E, since $\tau_{\max}$ is smaller than critical shear stress, e.g., τ_c, the TBE solution in or around the EDL flocculates, which is accompanied by a fast increase in $\tau_{\max}$ but a slow and nonlinear increase in $\gamma_{\max}$. In this state, the flow behaves rheologically. When E is sufficiently large, with $\tau_{\max} > \tau_c$, the interactions between the TBE molecules and the wall are broken. The cause of the shear-thickening effect, i.e., the flocculation of fluid particles in or around EDL is blocked and removed by EOF. Newtonian behavior with constant viscosity emerges again.

At present, to the best of the authors' knowledge, n is an experimental factor, and there is no theory that can predict it. The reason that n becomes maximum at pH = 7 is beyond the scope of this manuscript. However, we can try to explain this observation qualitatively by the relations between $\tau_{\max}$ and τ_c. From eq 23, it can be seen that $\tau_{\max}$ increases linearly with $|\zeta|$. Furthermore, τ_c is qualitatively proportional to the square of surface potential (Ψ_0) as $\tau_c \sim \Psi_0^2$,[17] with $\Psi_0 = \rho_{e_0}/C + \zeta$, where C is the capacity related to Ψ_0 and ζ, and ρ_{e_0} is the surface charge density. Both ζ and ρ_{e_0} are closely related to the pH value of the solution, as investigated by Behrens and Grier[18]

$$\zeta(\rho_{e_0}) = \frac{k_B T}{e}\left[\ln\left(\frac{-\rho_{e_0}}{e\Gamma + \rho_{e_0}}\right) - (\mathrm{pH} - \mathrm{p}K)\ln(10)\right] - \frac{\rho_{e_0}}{C} \tag{24}$$

DOI: 10.1021/acs.langmuir.8b03112
Langmuir XXXX, XXX, XXX−XXX

where $\Gamma = \Gamma_{SiO^-} + \Gamma_{SiOH}$ is the total site density, with Γ_{SiO^-} and Γ_{SiOH} representing the site density of SiO^- and SiOH, respectively, on the silica−water interface. ρ_{e_0} is the surface charge density given by $\rho_{e_0} = -e\Gamma_{SiO^-}$.[19] $C = \rho_{e_0}/(\Psi_0 - \zeta)$ is the capacity related to the surface potential (Ψ_0) and ζ. However, from the Poisson−Boltzmann equation, the following is also obtained[18,20]

$$\rho_{e_0}(\zeta) = \frac{\varepsilon k_B T \kappa}{2\pi e}\left[\sinh\left(\frac{e\zeta}{2k_B T}\right) + \frac{2}{\kappa R}\tanh\left(\frac{e\zeta}{4k_B T}\right)\right] \tag{25}$$

Here, we solve eqs 24 and 25 simultaneously with $\Gamma = 8$ nm^{-2} and $C = 2.9$ F/m^2 [20,21] in the experimental conditions of 0.7× TBE solution to investigate how ζ and ρ_{e_0} change with pH. The results are plotted in Figure 10. In general, both $|\zeta|$ and $|\rho_{e_0}|$ are monotonically increasing functions of pH. The difference is that in the considered range of pH, $|\zeta|$ increases linearly with pH, while $|\rho_{e_0}|$ increases nonlinearly with pH. Thus, $\tau_{max} \sim$ pH and $\tau_c \sim$ pH$^\alpha$ with $\alpha > 2$. In case $\tau_{max} < \tau_c$, a general equation

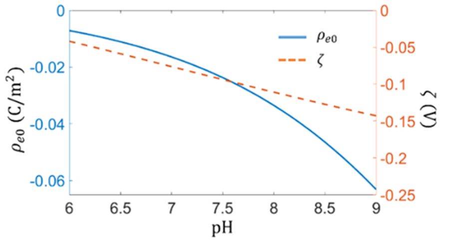

Figure 10. Variation in ζ and ρ_{e_0} with pH for 0.7× TBE solution.

$$f(\text{pH}) = \tau_c - \tau_{max} = A_1 \times \text{pH}^\alpha - A_2 \times \text{pH} + A_3 > 0 \tag{26}$$

must be satisfied, where A_1, A_2, and A_3 are coefficients irrelevant to pH. Since the actual variations in ζ and τ_c with respect to pH are more complicated, as investigated by Shan et al.,[22] A_1, A_2, and A_3 should be determined experimentally. As $\alpha > 2$, there must be a pH value, say pH$_p$, that corresponds to the peak of f(pH). In other words, at pH$_p$, it is more difficult to achieve $\tau_{max} > \tau_c$. Thereafter, a larger n can be predicted. From Figure 7, it can be seen that a maximum n is primarily observed at pH = 7 and secondarily observed at pH = 8. Both of the pH values are sufficiently close to the dissociation constant (pK), which is approximately 7.5 on the silica−water interface.[21] This implies that, in the investigation, pH$_p \approx$ pK.

The rheological behavior of TBE solution in nanofluidics under low electric fields has not been reported previously. However, this behavior may not be limited to TBE solutions; in fact, it may be a behavior commonly observed in nanofluidics and biomedical science. For example, in biophysics and bioengineering, the properties of biofluids are especially important in determining the behaviors of flows. Shear stress, ionic strength, cytoplasm viscosity, and the corresponding transport phenomena all play roles in regulating cell function and may even induce tumorization.[23−26] In electrophysiology, the mechanisms of injury currents are also an important topic and are related to nerve regeneration. For example, at the cut ends of the Mauthner and Muller axons in an embryonic lamprey spinal cord, an injury current of 100 μA/cm^2 with steady voltage gradients of 10 V/m was measured.[27] Further investigations have shown that the regeneration of cut axons can be promoted by applying an inverse voltage.[28,29] Injury currents and reverse currents for regeneration occur in nanoscale channels with voltage gradients on the order of 10 V/m. These phenomena are located in the parameter ranges of this investigation. The shear-thickening effect observed in the investigation may reveal that the transport of ions accompanied by injury currents could be faster than that conventionally believed. With proper adjustment of the flow behavior index of the medium, nerve regeneration could be further promoted by applying reverse voltage.

Furthermore, the rheological behavior of solutions under low electric fields is also essential when designing nanofluidic chips, especially in electroosmosis-based DNA analysis techniques. We hope that this investigation will significantly promote the development of nanofluidic chips when electrokinetic mechanisms are used for controlling flow and the movement of samples.

■ ASSOCIATED CONTENT

Ⓢ Supporting Information

The Supporting Information is available free of charge on the ACS Publications website at DOI: 10.1021/acs.langmuir.8b03112.

Nonlinear fittings of the flow behavior indices on experimental data are plotted and summarized (PDF)

■ AUTHOR INFORMATION

Corresponding Authors

*E-mail: zhao9@email.sc.edu (W.Z.).
*E-mail: wangkg@nwu.edu.cn (K.W.).

ORCID

Jing Xue: 0000-0002-1896-265X
Wei Zhao: 0000-0002-3370-6216
Guiren Wang: 0000-0002-5379-0814
Junjie Li: 0000-0002-1508-9891

Notes

The authors declare no competing financial interest.

■ ACKNOWLEDGMENTS

This work was supported by the National Natural Science Foundation of China (Grant No. 61378083, 11672229, 61405237), the International Cooperation Foundation of the National Science and the Technology Major Project of the Ministry of Science and Technology of China (Grant No. 2011DFA12220), the Major Research Plan of the National Nature Science Foundation of China (Grant No. 91123030), the Natural Science Foundation of China (Grant Nos. 2010JS110, 14JS106, 14JS107, and 2013SZS03-Z01), the Natural Science Foundation of the Education Department of the Shaanxi Provincial Government (No. 17JK0760), the Natural Science Basic Research Program of Shaanxi Province—Major Basic Research Project (2016ZDJC-15, S2018-ZC-TD-0061), and the Natural Science Foundation of Jiangsu Province (Grant No. BK20140379).

■ REFERENCES

(1) Whitby, M.; Quirke, N. Fluid flow in carbon nanotubes and nanopipes. *Nat. Nanotechnol.* **2007**, *2*, 87−94.

(2) Pfahler, J.; Harley, J.; Bau, H. H.; Zemel, J. N. Liquid transport in micron and submicron channels. *Sens. Actuators, A* **1990**, *22*, 431−434.

(3) Majumder, M.; Chopra, N.; Andrews, R.; Hinds, B. J. Nanoscale hydrodynamics: enhanced flow in carbon nanotubes. *Nature* **2005**, *438*, No. 44.

(4) Stein, D.; Kruithof, M.; Dekker, C. Surface-charge-governed ion transport in nanofluidic channels. *Phys. Rev. Lett.* **2004**, *93*, No. 035901.

(5) Kneller, A. R.; Haywood, D. G.; Jacobson, S. C. AC Electroosmotic Pumping in Nanofluidic Funnels. *Anal. Chem.* **2016**, 6390−6394.

(6) Liu, W. K.; Tebbs, S. E.; Byrne, P. O.; Elliott, T. S. The effects of electric current on bacteria colonising intravenous catheters. *J. Infection* **1993**, *27*, 261−269.

(7) Jain, S.; Sharma, A.; Basu, B. Vertical electric field stimulated neural cell functionality on porous amorphous carbon electrodes. *Biomaterials* **2013**, *34*, 9252−9263.

(8) Duan, Y.; Zhao, W.; Xue, J.; Sun, D.; Wang, K.; Wang, G.; Li, J.; Bai, J.; Gu, C. Current characteristics of λ-DNA molecules/polystyrene nanoparticles in TBE buffer solution through micro/nanofluidic capillaries under DC electric field. *J. Phys. D: Appl. Phys.* **2017**, *50*, No. 125401.

(9) Sheng, P.; Wen, W. Electrorheological Fluids: Mechanisms, Dynamics, and Microfluidics Applications. *Annu. Rev. Fluid Mech.* **2012**, *44*, 143−174.

(10) Huang, C. C.; Chiu, T. C.; Chang, H. T. Effects of metal ions on concentration of DNA in high-conductivity media by capillary electrophoresis. *J. Chromatogr. A* **2002**, *966*, 195−203.

(11) Irgens, F. *Rheology and Non-Newtonian Fluids*; Springer: Berlin, 2014; pp 15−26.

(12) Singh, K. P.; Guo, C. Current-voltage characteristics influenced by the nanochannel diameter and surface charge density in a fluidic field-effect-transistor. *Phys. Chem. Chem. Phys.* **2017**, *19*, 15701−15708.

(13) Keh, H. J.; Liu, Y. C. Electrokinetic flow in a circular capillary with a surface charge layer. *J. Colloid Interface Sci.* **1995**, *172*, 222−229.

(14) Kirby, B. J. *Micro- and Nanoscale Fluid Mechanics: Transport in Microfluidic Devices*; Cambridge University Press: NY, 2010.

(15) Morrison, I. D.; Ross, S. *Colloidal Dispersions: Suspensions, Emulsions, and Foams*; Wiley, 2002.

(16) Feng, G.; Huang, J.; Sumpter, B. G.; Meunier, V.; Qiao, R. Structure and dynamics of electrical double layers in organic electrolytes. *Phys. Chem. Chem. Phys.* **2010**, *12*, 5468−5479.

(17) Maranzano, B. J.; Wagner, N. J. The effects of particle size on reversible shear thickening of concentrated colloidal dispersions. *J. Chem. Phys.* **2001**, *114*, 10514−10527.

(18) Behrens, S. H.; Grier, D. G. The charge of glass and silica surfaces. *J. Chem. Phys.* **2001**, *115*, 6716−6721.

(19) Behrens, S. H.; Borkovec, M. Electrostatic Interaction of Colloidal Surfaces with Variable Charge. *J. Phys. Chem. B* **1999**, *103*, 2918−2928.

(20) van der Heyden, F. H. J.; Stein, D.; Dekker, C. Streaming Currents in a Single Nanofluidic Channel. *Phys. Rev. Lett.* **2005**, *95*, No. 116104.

(21) Hiemstra, T.; Van Riemsdijk, W. H.; Bolt, G. H. Multisite proton adsorption modeling at the solid/solution interface of (hydr)oxides: A new approach: I. Model description and evaluation of intrinsic reaction constants. *J. Colloid Interface Sci.* **1989**, *133*, 91−104.

(22) Shan, L.; Tian, Y.; Jiang, J.; Zhang, X.; Meng, Y. Effects of pH on shear thinning and thickening behaviors of fumed silica suspensions. *Colloids Surf., A* **2015**, *464*, 1−7.

(23) Bruno, S.; Gorczyca, W.; Darzynkiewicz, Z. Effect of ionic strength in immunocytochemical detection of the proliferation associated nuclear antigens p120, PCNA, and the protein reacting with Ki-67 antibody. *Cytometry* **1992**, *13*, 496−501.

(24) Gerweck, L. E.; Seetharaman, K. Cellular pH gradient in tumor versus normal tissue: potential exploitation for the treatment of cancer. *Cancer Res.* **1996**, *56*, 1194−1198.

(25) Voets, T.; Droogmans, G.; Raskin, G.; Eggermont, J.; Nilius, B. Reduced intracellular ionic strength as the initial trigger for activation of endothelial volume-regulated anion channels. *Proc. Natl. Acad. Sci. U.S.A.* **1999**, *96*, 5298−5303.

(26) Krizkova, S.; Fabrik, I.; Adam, V.; Kukacka, J.; Prusa, R.; Trnkova, L.; Strnadel, J.; Horak, V.; Kizek, R. Effects of Reduced Glutathione, Surface Active Agents, and Ionic Strength on the Detection of Metallothioneins by Using of Brdicka Reaction. *Electroanalysis* **2009**, *21*, 640−644.

(27) Borgens, R. B.; Jaffe, L. F.; Cohen, M. J. Large and persistent electrical currents enter the transected lamprey spinal cord. *Proc. Natl. Acad. Sci. U. S. A.* **1980**, *77*, 1209−1213.

(28) Borgens, R. B.; Roederer, E.; Cohen, M. J. Enhanced spinal cord regeneration in lamprey by applied electric fields. *Science* **1981**, *213*, 611−617.

(29) Borgens, R. B.; Metcalf, M. E.; Blight, A. R. Delayed application of direct current electric fields in experimental spinal cord injuries. *Restor. Neurol. Neurosci.* **1993**, *162*, 1−7.